Eur. Phys. J. Special Topics **227**, 2617–2640 (2019)

https://doi.org/10.1140/epjst/e2019-800135-2

THE EUROPEAN PHYSICAL JOURNAL SPECIAL TOPICS

Regular Article

Understanding nonlinearity in electrochemical systems

Nicolas Wolff[1,2,a], Nina Harting[1,2], Fridolin Röder[1], Marco Heinrich[1,2,3], and Ulrike Krewer[1,2]

[1] Institute of Energy and Process Systems Engineering, TU Braunschweig, Braunschweig, Germany
[2] Battery LabFactory Braunschweig, TU Braunschweig, Braunschweig, Germany
[3] Physikalisch Technische Bundesanstalt, Braunschweig, Germany

Received 26 August 2018 / Received in final form 26 December 2018
Published online 17 April 2019

Abstract. Commonly applied electrochemical methods for the analysis and diagnosis of the processes in and state of electrochemical cells, such as Electrochemical Impedance Spectroscopy and Current Interrupt analysis, are either limited to linear analysis or the signal is quite unspecific which hampers to extract significant and precise nonlinear information. We present a systematic insight into how significant information can be extracted from a promising alternative nonlinear dynamic electrochemical analysis technique, Nonlinear Frequency Response Analysis. Further, we present a fundamental and in-depth study of impact of processes at electrodes on nonlinear behavior. Model based analysis of a reaction process with Butler-Volmer kinetics and of a diffusion process are thereby used to understand and interpret the excitation of higher harmonics. A reaction with a symmetric current potential relation thereby causes an excitation of the third harmonic, whereas for the diffusion process the second and third harmonic are excited. Nonlinearities caused by diffusion are limited to low frequencies. Further, parameter variations of exchange current density, double layer capacitance and diffusion coefficient as well as variation of the input signal show that the symmetry of the nonlinear behavior between current and potential is responsible for the excitation of the second and third harmonic. The tangent method is presented as a suitable method to quantitatively evaluate and compare influences of each process and parameter on spectrum features and the related characteristic frequency range. The work thus serves as a guideline for using and interpreting nonlinear frequency response spectra.

1 Introduction

Safety and performance of electrochemical technologies, such as batteries, electrolysers and fuel cells is essential to accelerate the change towards green and renewable energies and towards sustainable production of chemicals via power-to-x. To fulfil

[a] e-mail: n.wolff@tu-braunschweig.de

this ambitious goal, exact characterization of processes within the previously mentioned cells and their electrodes is needed. Dynamic electrochemical analysis offers the advantage to separate slow from fast processes, and thus an in-depth study and more information of single processes, compared to steady state techniques such as Tafel slope interpretation. It is thus frequently applied in electrochemistry [3,18]. Currently, one of the most popular dynamic electrochemical analysis and state diagnosis methods is EIS. This analysis technique is limited to a linear excitation of the investigated system.

Nevertheless, processes within electrochemical cells such as the electrochemical reaction are nonlinear processes [16,27] and can show complex nonlinear behavior, i.e. spontaneous oscillation of current or potential [15] and if EIS is applied, not all useful information can be accessed [8]. In this case, characterization of processes would benefit from a nonlinear dynamic measurement method, such as Nonlinear Frequency Response Analysis (NFRA). Here, higher harmonics accessed by a sinusoidal deflection with a large amplitude are used for process identification and characterization [24]. Other nonlinear techniques are Cyclovoltammetry (CV) and Chronoamperometry (CA) or -potentiometry (CP). CV is usually employed for in-depth study of reaction and sorption processes at single electrodes or for material characterization regarding performance, active area and stability [9,25]. It thus often focuses on surface processes studied on plain electrodes in solutions, but it is seldomly applied to full cells, as transport processes make signal interpretation difficult [6,9]. Also CA or CP are frequently applied for material characterization and kinetic studies. The method is also applied to full cells, e.g. as Current Interrupt (CI) analysis for determining Ohmic resistance in fuel cells or batteries [5,26], or to study the interaction of reaction, sorption and transport processes at electrode or cell level [3,17]. Dynamic electrochemical methods may be coupled with physical or chemical methods, e.g. as done in Differential Electrochemical Mass Spectroscopy (DEMS) [2,19]. However, CV, CA and CP are less suitable or accurate for separating and separate analysis of fast and slow processes. Here, frequency response analysis as in Electrochemical Impedance Spectroscopy (EIS) and Nonlinear Frequency Response Analysis (NFRA) has its advantages, as the results are given over a wide frequency range from mHz to MHz.

NFRA has been applied to study the nonlinear behavior of ferrocyanide oxidation using a mathematical model [28] and measurements [29]. An additional implementation of NFRA to access nonlinearities in impedance spectra, and further to sense and determine reaction kinetics in an electrochemical cell was investigated by Kiel et al. [14]. Later research focuses on the application of NFRA to electrochemical methanol oxidation using Volterra series. They found that the linear output (EIS) does not contain sufficient information to discriminate between different kinetic models, but NFRA however does [4]. Kadyk et al. further investigated the CO poisoning and dehydration within a PEM fuel cell, using experiments and simulations. The model approach is again based on a Volterra series. They thereby found that CO poisoning can be detected with NFRA due to a change in the second order response, but not with conventional methods such as EIS [11–13]. Additionally, NFRA was used to identify reaction kinetics of methanol oxidation [22] and oxygen reduction [21] in model based and experimental studies on fuel cells and further for state estimation as well as methanol concentration sensing of a fuel cell [20]. A further study of the excitation higher harmonic voltage responses was investigated by Wilson et al., on solid oxide fuel cells, thereby showing that higher harmonic voltage responses contain specific resonant features [30]. In the field of Lithium-ion batteries, Harting et al. were the first to show the experimental application of NFRA and to use it to discriminate between different processes in cells [8] and between different degradation processes [7]. Further research focused on an application of NFRA on a pseudo-two-dimensional battery model to enhance the interpretation of NFR spectra [31] and a

base case study to explore the effect of kinetic, mass-transport and thermodynamic parameters on the harmonics response [23].

The previous analyses focused on optimal usage of NFRA for a given application, e.g. how to correlate a spectrum feature to a certain process or variable in a complex system. In general, despite the obvious advantages, very few groups use this technique, and the method has not yet entered electrochemical textbooks, nor is it widely known. Whereas several of the leading laboratory EIS measurement device suppliers nowadays feature this technology as a free option, researchers may be discouraged by the yet difficult interpretation of the observed features in the spectra. A systematic fundamental analysis of single processes and their impact on NFR spectra is missing, which prevents wide-spread application of this promising, advanced, but yet not well understood characterization technique. Such a systematic and generic, i.e. application-independent analysis will deliver a sound knowledge base and guideline which experts and newcomers can use for their application specific analyses.

Within this research, we aim to deliver such a basic guideline to enhance interpretation and usage of NFRA via illustrating the nonlinearity using simple fundamental models. The effect of fundamental processes in electrochemical cells on NFR spectra is first analyzed using a most basic electrochemical reaction. Subsequently, the often encountered limited reactant availability, due to slow diffusion, is analyzed, and their impact on NFR is shown. Then the interaction of both processes is studied. In addition, analysis of sensitivity of the spectra to electrode parameters gives the reader an idea on how parameters and their changes, e.g. due to ageing, impact the spectra. In detail, a variation of characteristic parameters, such as double layer capacitance, excitation amplitude and exchange current density, is conducted.

2 Method

In contrast to the commonly applied EIS, the electrochemical cell is nonlinearly excited for NFRA to access higher harmonic responses. The fundamental working principle of NFRA is schematically shown in Figure 1.

A sinusoidal current with high AC excitation amplitude is applied to the electrochemical cell or electrode. The dynamic output signal of the voltage to the current input with frequency f_1 contains besides a sinusoidal voltage response with amplitude Y_1 with the inlet frequency f_1 also sinusoidal voltage responses of amplitude Y_n with n times the input frequency $f(Y_n) = n \cdot f_1$. To extract and analyze these higher frequency responses from the output voltage signal, it is transferred from the time domain to the frequency domain via a fast Fourier transformation (FFT). This allows to display higher frequency responses Y_n as a function of the input frequency f_0, as shown as an example for the discrete Fourier-transformation in equation (1)

$$Y_n = |\frac{2}{z}\sum_{j=0}^{z-1} v_j \left[\cos(2\pi f_0 nj) - i\sin(2\pi f_0 nj)\right]| = |\frac{2}{z}\sum_{j=0}^{z-1} v_j e^{-i2\pi f_0 nj}|, \qquad (1)$$

with z as the number of sample points, v_j as the calculated discrete output voltage of the model in the time domain and n as the numerator for higher harmonic voltage responses. The amplitudes of these higher frequency responses, the so called higher harmonics Y_n, are further used for process characterization. Additional in-depth descriptions of the method are found in our previous publications [7,8,11,31]. Please note that there are also other options to analyze the nonlinear frequency response, e.g. via Volterra series, which also yield phase shifts. However, we here use an approach based on the widely applied method of total harmonic distortion, which

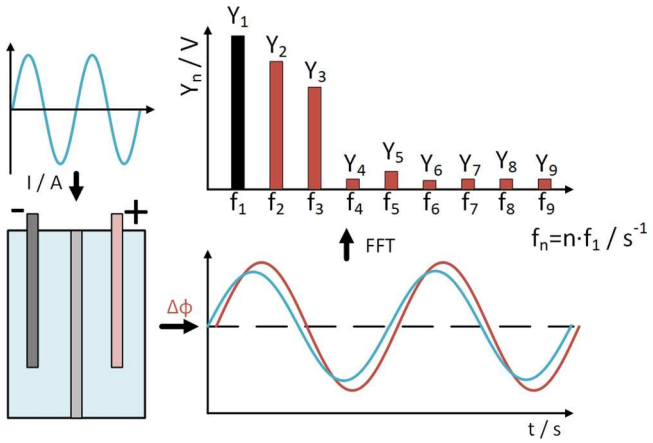

Fig. 1. Schematic illustration of the working principle of NFRA.

analyses only the amplitude [22]. It should be noted, that in contrast to total harmonic distortion or also electrochemical impedance spectroscopy, we do not normalize the voltage response. This allows electrochemists to better practically interpret the response signal. Within this research, the second Y_2 and third Y_3 individual harmonics as well as the root mean square of the first two harmonics Y_{rms} shown in equation (2), are used

$$Y_{\mathrm{rms}} = \sqrt{\frac{\sum_{i=2}^{3} Y_n^2}{2}}. \tag{2}$$

We use the root mean square (rms) instead of the sum of all higher harmonics, or the square root of the squares of the higher harmonics, which we used in past work [7,8,31], because the rms is a well known measure in metrology and electrical engineering, also for total harmonic distortion [22], and it gives a sound mean value of overall nonlinearity of a system. As the rms requires division by the number of higher harmonics, comparability of rms values will be only given if the same number of higher harmonics is used. As explained in the following, we recommend Y_2 and Y_3. The amplitudes are chosen so that nonlinear responses for Y_2 and Y_3 are visible, but all further higher harmonics, i.e. $n > 3$ are negligible. This prevents interference of the signals [29]. Please note that, if the excitation signal contains nonlinearities, all harmonics can be influenced. Further, 20 continuous sinusoidal cycles are calculated in this study and the data is extracted from the last cycle to guarantee the dynamic equilibrium of the system. We used the function fft implemented in Matlab to extract the amplitude.

2.1 Tangent method

Changes of parameters can significantly influence NFR spectra. Therefore, we want to introduce a method which can be generally applicable to gather and compare characteristic values of the spectra. In our case, this method is the tangent method.

The tangent method is a standard technique in control engineering for identification and analysis of dynamic systems. Control parameters, respectively characteristic values, of the system are gained using the tangent method. Characteristic time periods

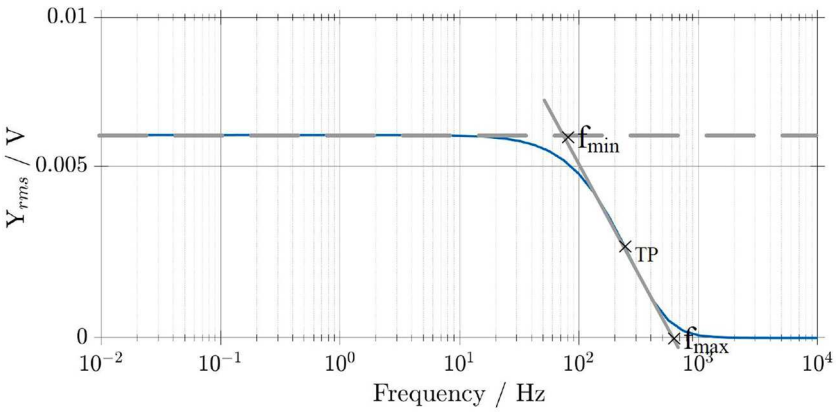

Fig. 2. Tangent method for simulated Y_{rms} with the reference case simulation parameters from Table 1.

of the control system are identified with this method. As the shape of a NFR spectrum resembles the typical shape of a step response of a dynamic control system, the tangent method is applied in this study for the characterization of NFR spectra. The tangent method is used for each suitable simulation for the calculation of characteristic parameters of NFRA, shown in Figures 11, 12 and 13. Thereby, the characteristic frequencies $f_{\max}$, $f_{\min}$ and the turning point TP, which identify and separate specific regions in the NFRA, are recorded, as shown in Figure 2.

3 Mathematical modeling

Focus of this research is laid on the understanding of the excitation of higher harmonics. Therefore, a reaction process according to Butler-Volmer kinetics and a diffusion process according to Fick's law are investigated in a model based approach. For the sake of simplicity, we ignore further mass transport processes, such as migration, convection and electro-osmotic drag, heat transport as well as complex surface processes and adsorption or desorption.

All functions used within this work are embedded in Matlab, the spatial discretization of the partial differential equations used for simulating diffusion is implemented with a finite volume approach, and time derivatives are solved with an ode-solver. A spatial discretization is chosen that is sufficiently fine to guarantee a mesh independent solution. Computation time was typically below 15 min. A base case parameter set is provided in Table 1, with the initial concentration of reactant A $c_{A,0}$, the specific surface area a_s. Further, reference values for double layer capacitance $C_{\mathrm{DL},0}$, exchange current density $i_{0,0}$, symmetry factor α, diffusion coefficient D_0, AC current density $I_{\mathrm{AC},0}$, thickness d as well as ambient temperature T are used in this study.

Since this model based study targets to explain the fundamentals of the excitation of higher harmonic voltage responses, a one step redox reaction is assumed as a base case scenario:

$$\mathrm{A} \rightleftharpoons \mathrm{A}^{+} + \mathrm{e}^{-}. \tag{3}$$

An unlimited reservoir for A^{+} and a constant activity of 1 are assumed. The reservoir of A on the other hand is limited. A change of its activity a_A leads to a change of the open circuit potential of the system $\Delta\phi^0$, implemented via a Nernst-approach, given

Table 1. Simulation parameters.

Parameters	Value	Unit
$c_{A,0}$	1.5×10^4	mol m^{-3}
a_s	1.5×10^5	m^{-1}
$C_{\mathrm{DL},0}$	0.2	F m^{-2}
$i_{0,0}$	10	A m^{-2}
α	0.5	–
D_0	1.0×10^{-12}	m^2 s^{-1}
$I_{\mathrm{AC},0}$	400	A m^{-2}
d	50.0×10^{-6}	m
T	300	K

in equation (4). This activity dependence of the potential is measured to a neutral reference and for the simple priorly described redox reaction it can be expressed as follows:

$$\Delta\phi^0 = \Delta\phi^{00} + \frac{\mathrm{R}T}{\mathrm{F}} \ln \frac{1}{a_A}, \tag{4}$$

with the standard potential $\Delta\phi^{00}$, Faraday constant F, ideal gas constant R and temperature T. The activity a_A can be expressed by the corresponding concentration c_A and its standard equilibrium concentration $c_{A,0}$, if an ideal system with an activity coefficient of one is investigated, as shown in the following:

$$a_A = \frac{c_A}{c_{A,0}}, \tag{5}$$

with

$$\Delta\phi^0 = \Delta\phi^{00} + \frac{\mathrm{R}T}{\mathrm{F}} \ln \frac{1}{\frac{c_A}{c_{A,0}}}. \tag{6}$$

The priorly described one step reaction, shown in equation (3), can be modeled via a Butler-Volmer equation, which, according to Bard et al. [3], further can be expressed as follows, including the already made assumptions:

$$j_{\mathrm{f}} = a_s i_0 \left(\frac{c_A}{c_{A,0}} \exp\left(\alpha \frac{\eta \mathrm{F}}{\mathrm{R}T} \right) - \exp\left(-(1-\alpha) \frac{\eta \mathrm{F}}{\mathrm{R}T} \right) \right), \tag{7}$$

with the Faradaic volumetric reaction current j_{f}, specific surface area of the electrode a_s, exchange current density i_0 and overpotential η.

The overpotential η used in the previous equation is defined as:

$$\eta = \Delta\phi - \Delta\phi^0, \tag{8}$$

with the potential gradient across the interface $\Delta\phi$.

Additionally to the ion generation rate due to Butler-Volmer kinetics, a total volumetric current j_{tot} leaves or enters the interface, resulting in the charge balance:

$$a_s \cdot C_{\mathrm{DL}} \frac{\partial \Delta\phi}{\partial t} = j_{\mathrm{tot}} - j_{\mathrm{f}}, \tag{9}$$

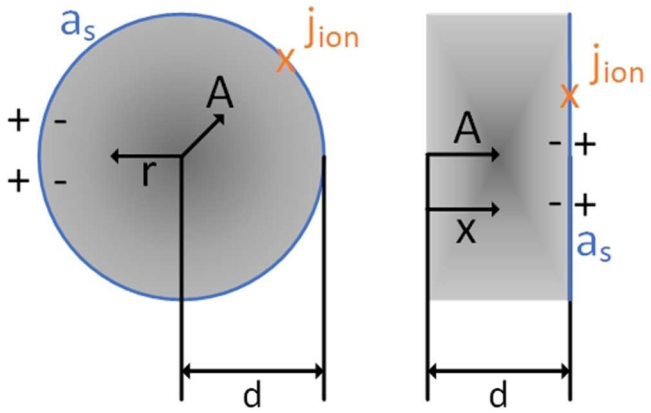

Fig. 3. Schematic illustration of the implemented spherical diffusion and planar diffusion of species A to the electrochemically active surface (blue), where the reaction j_f takes place.

with the electric double layer capacitance C_{DL}. The current per electrode volume j_{tot}, thereby equals the externally applied sinusoidal current per geometric area of electrode per electrode thickness d with amplitude I_{AC}, as shown in the following equation:

$$j_{\mathrm{tot}} = \frac{I_{\mathrm{AC}}}{d} \sin(2\pi f t). \tag{10}$$

As species are consumed or produced at the interface, reactant and product species need to diffuse to or from the interface before or after reaction, respectively. If, a volumetric current is transferred to a current across an interface, the specific surface area a_s is used. Diffusion impacts the concentration at the surface, and by this both, the overpotential, e.g via a concentration dependent Butler-Volmer curve, i.e, kinetics, and the open circuit potential via the Nernst equation. Both, open circuit potential and overpotential impact electrode potential and thus dynamic response of potential to current.

Typical diffusion processes in cells are planar diffusion, e.g. occurring between the electrodes in the electrolyte, or spherical diffusion in spherical electrode particles, as observed in insertion electrodes of batteries, such as Lithium-ion batteries, where the reduced species is stored and diffuses in the active material particles. Diffusion processes are implemented according to Fick's law. Within this research, we investigate differences between planar and spherical diffusion, shown in equations (11) and (12), respectively

$$\frac{\partial c_A}{\partial t} = \frac{\partial}{\partial x}\left(D \frac{\partial c_A}{\partial x}\right), \tag{11}$$

$$\frac{\partial c_A}{\partial t} = \frac{1}{r^2}\frac{\partial}{\partial r}\left(D r^2 \frac{\partial c_A}{\partial r}\right), \tag{12}$$

with the time t, diffusion coefficient D and spacial coordinates x and r, respectively. Concerning planar and spherical diffusion, a maximal diffusion length, which corresponds to the thickness d, is set, respectively. In Figure 3, a schematic illustration of the implemented spherical and planar diffusion with the corresponding diffusion length d is shown.

Boundary conditions are provided in the following:

$$\frac{\partial c(0)}{\partial r} = \frac{\partial c(0)}{\partial x} = 0, \frac{\partial c(d)}{\partial r} = \frac{\partial c(d)}{\partial x} = \frac{j_\mathrm{f}}{Da_s F}. \tag{13}$$

3.1 Model for impact of reaction process

In a first step, focus is laid on an investigation of the reaction process and the nonlinear response of $\Delta\phi$. For this purpose, influences of concentration changes are fully neglected. Therefore c_A is assumed to be constant and the previously derived and described equations can be simplified as follows.

For the Nernst-equation, shown in equation (4), a constant concentration c_A leads to a constant open circuit potential $\Delta\phi^0$:

$$\Delta\phi^0 = \Delta\phi^{00} = \text{constant}. \tag{14}$$

Additionally within the Butler-Volmer equation, shown in (7) the priorly concentration dependent forward reaction can be simplified to a concentration independent reaction:

$$j_\mathrm{f} = a_s i_0 \left(\exp\left(\alpha \frac{\eta \mathrm{F}}{\mathrm{R}T} \right) - \exp\left(-(1-\alpha) \frac{\eta \mathrm{F}}{\mathrm{R}T} \right) \right). \tag{15}$$

All other equations remain valid without simplifications.

3.2 Model for impact of diffusion process

In a second step, we aim to understand in-depth the excitation of higher harmonics due to diffusion. We use the model as it was derived in Section 3, without further simplifications. However, to isolate the influence of the diffusion process, at this point, we neglect the effect of reaction via Butler-Volmer kinetics, i.e. η on the nonlinear response and analyze the higher harmonic voltage response of $\Delta\phi^0$. While we analyze both, spherical and planar diffusion, we define spherical diffusion as the reference scenario.

3.3 Model for impact of coupled processes

In a last step, the interaction and coupling of reaction and spherical diffusion are investigated as they are inevitably coupled in electrochemical systems. Also, the diffusion impact on η will be elucidated. Here, the complete model, derived in Section 3, without further simplifications is used.

4 Results and discussion

In-depth understanding of the excitation of higher harmonics is generated and discussed within this research. For this purpose, the root mean square Y_rms, calculated with the first two higher harmonics Y_{2-3} as well as individual harmonics Y_2 and Y_3 are investigated, as previously stated; impedance spectra, calculated with small excitation amplitude, are provided where helpful for the discussion. First, the reaction

process is analyzed, then different diffusion processes are investigated followed by a coupling of reaction and diffusion. To quantitatively evaluate and compare the spectra characteristic, parameter specific information gathered from the tangent method are shown and discussed. The tangent method is described in Figure 2 in Section 2.1. We are aware that multiple possibilities to quantify changes in spectra exist. Nevertheless, in our opinion, the tangent method is a suitable method to gather characteristic frequencies and intensities of these spectra and evaluate changes in the symmetry.

4.1 Impact of reaction

In this first section, we aim to systematically and thoroughly characterize the priorly described reaction process. Therefore the general model from Section 3 with the simplification from Section 3.1 is used. In Figure 4, simulations with the base case parameter set given in Table 1 and a variation of the AC excitation amplitude between 0.5 $I_{AC,0}$ and 2.0 $I_{AC,0}$ are shown. If not mentioned otherwise, the base case parameters are chosen for simulation. The NFR spectrum with an excitation amplitude of 1.0 $I_{AC,0}$ is referred to as reference simulation in the following and is marked with an asterisk. Additional to NFR simulations, EIS, simulated with an excitation amplitude of 0.1 $I_{AC,0}$, guaranteeing linear behavior of the system, is provided. In Figure 4a, three frequency ranges with characteristic nonlinearities are identified for Y_{rms}, applying the tangent method, described in Section 2.1. The general shape resembles that of a bode plot of an EIS, its high frequency value being zero and low frequency value being constant. For high frequencies greater than the characteristic frequency f_{max} of 600 Hz (dash-dotted line in Fig. 4a), NFR have negligible intensity. In the frequency range below 600 Hz up to the second characteristic frequency f_{min} of 75 Hz (dashed line in Fig. 4a), NFR increase monotonously. One additional characteristic feature is identified in this frequency range, the turning point (TP) of the spectrum at 240 Hz (see blue circle in Fig. 4a). The characteristic frequency of the turning point is marked in each NFR spectrum in the corresponding plot color. For frequencies smaller than 75 Hz, NFR have an almost constant value of $Y_{rms}(f_{min})$. As f_{min} and f_{max} separate the three characteristic frequency regions, we use them in the following to separate and separately discuss the three regions in-depth. The three characteristic features, namely f_{max}, f_{min} as well as $Y_{rms}(f_{min})$, are identified for each simulated parameter variation concerning the reaction process for the root mean square Y_{rms} and shown in Figures 11, 12 and 13 at the end of this section. The change of these characteristic features in dependence of the specific parameter variations is discussed and concluded on at the end of this section, as well. In Figure 4b, the individual higher harmonics Y_2 and Y_3 are analyzed. Hereby, it is highly interesting to notice that only the third harmonic Y_3 is excited in the overall frequency range. The second harmonic Y_2, however, is not excited. Thus, it is deduced that one single electrochemical reaction implemented as previously described only impacts the third harmonic Y_3. Further, the same three characteristic frequency ranges as well as the same frequencies of the features f_{min}, f_{max} and TP, as for Y_{rms} are identified for the individual higher harmonic Y_3. In the additionally provided impedance spectrum, shown in Figure 4c, a semi circle corresponding to the electrochemical reaction with a characteristic frequency of 320 Hz, also marked for the NFR spectrum (black line), can be seen. This is in agreement to the literature [1].

In the following, the focus is laid on a qualitative description and analysis of the impact of the particular parameters on the NFR spectra, such as the excitation amplitude.

Increasing the sinusoidal excitation amplitude impacts Y_{rms}, shown in Figure 4a, as well as the individual higher harmonics, shown in Figure 4b. For the higher AC excitation of 2.0 $I_{AC,0}$, f_{min}, f_{max} shift towards higher frequencies and

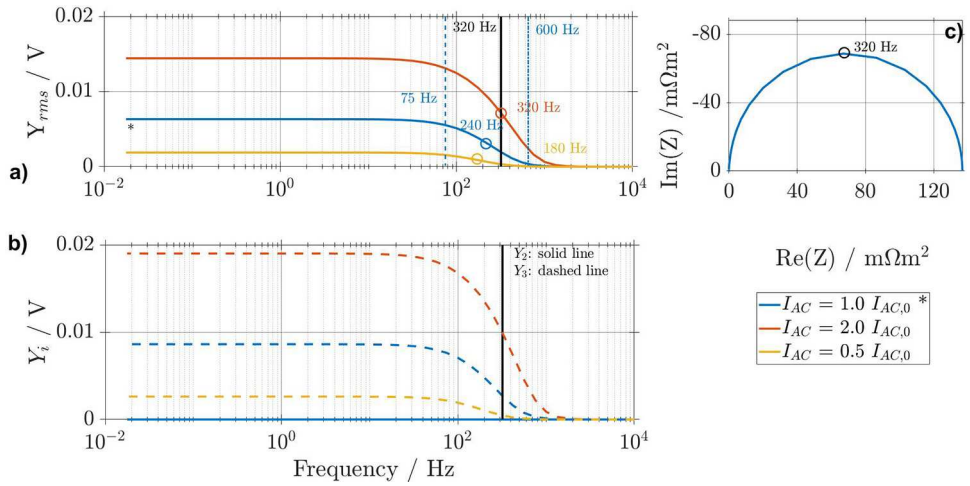

Fig. 4. Simulated NFR for the reaction model with a variation of the AC excitation amplitude for (a) Y_{rms}, (b) individual harmonics Y_2 and Y_3 and (c) EIS. The reference case simulation with parameters from Table 1 is marked with an asterisk. f_{min} is marked by a dashed blue line and f_{max} is marked by a dash-dotted blue line, both for the reference case simulation.

$Y_{\mathrm{rms}}(f_{\mathrm{min}})$ increases due to higher nonlinearities for the higher excitation amplitude. The characteristic frequency of TP shifts from 240 Hz for an excitation of 1.0 $I_{\mathrm{AC},0}$ to 320 Hz for 2.0 $I_{\mathrm{AC},0}$. If the excitation amplitude is lowered to 0.5 $I_{\mathrm{AC},0}$, f_{min}, f_{max} shift towards lower frequencies and $Y_{\mathrm{rms}}(f_{\mathrm{min}})$ decreases due to lower nonlinearities. The characteristic frequency of TP shifts from 240 Hz for an excitation of 1.0 $I_{\mathrm{AC},0}$ to 180 Hz for 0.5 $I_{\mathrm{AC},0}$. Therefore, a dependency of the characteristic features of the spectra on AC excitation amplitude can be deduced from this study for the simple reaction model. However, amplitude changes excite no novel characteristic features or qualitative change in the NFR spectrum. In Figure 4b, the individual higher harmonics Y_2 and Y_3 are analyzed for an increased AC amplitude. Increasing the AC excitation increases the intensity of the third harmonic as well $Y_{\mathrm{rms}}(f_{\mathrm{min}})$ and increases the characteristic frequencies, as well but does not lead to an excitation of Y_2.

Understanding the features of the NFR spectra and their dependence on the single processes is essential for a sound future interpretation of such spectra. As the best way to see the impact of single processes is by accelerating or slowing down each process via changing of its parameters, we conduct a systematic parameter sensitivity study in the following.

Based on the above given reference NFR simulation at 1.0 $I_{\mathrm{AC},0}$, parameter variations, for the double layer capacitance C_{DL} as well as the exchange current density i_0, are shown. Further, the influence of the symmetry factor α is investigated. DC currents or cell potentials that lead to a reaction and current are frequently used in EIS research to characterize the cell and processes under operation. Therefore, the impact of an additional DC current and its impact on NFR spectra is also elucidated.

In Figure 5, the influence of a variation of the double layer capacitance C_{DL} on Y_{rms} and EIS is shown. With increasing double layer capacitance C_{DL}, the dynamic answer of the reaction becomes slower and the characteristic frequencies f_{min} and f_{max} shift towards lower frequencies. Overall, this shift is linear, as it can be seen for the frequency of the turning point. This is similar to EIS simulations. By changing the double capacitance C_{DL} with one order of magnitude, the frequency of the turning point also shifts by one order of magnitude.

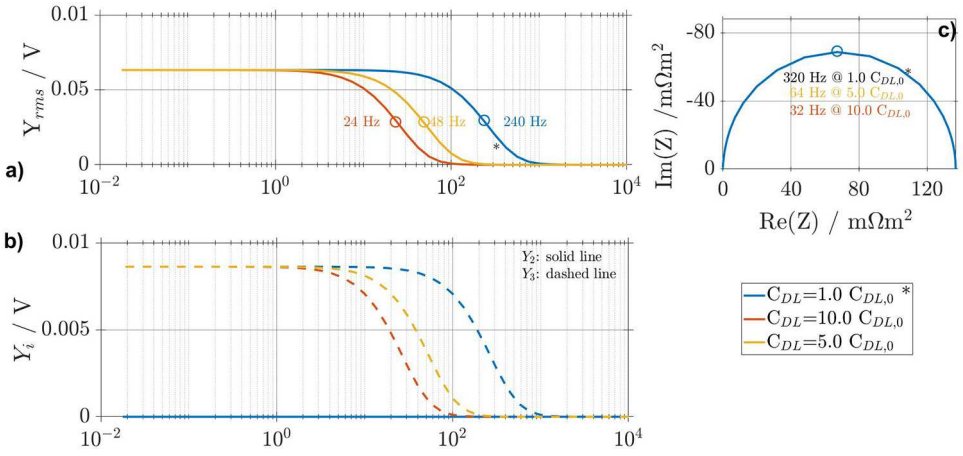

Fig. 5. Simulated NFR for the reaction model with a variation of the double layer capacitance C_{DL} and AC excitation amplitude for (a) Y_{rms}, (b) individual harmonics Y_2 and Y_3 and (c) EIS. The reference case simulation with parameters from Table 1 is marked with an asterisk.

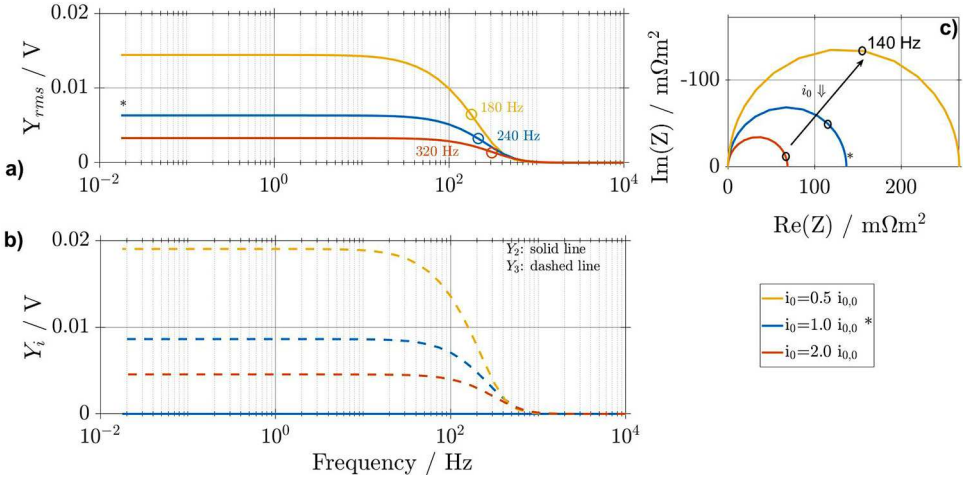

Fig. 6. Simulated NFR for the reaction model with a variation of the exchange current density i_0 for (a) Y_{rms}, (b) individual harmonics Y_2 and Y_3 and (c) EIS. The reference case simulation with parameters from Table 1 is marked with an asterisk.

Whereas the double layer capacitance C_{DL} impacts the characteristic frequency range of the reaction process in the spectra, it does not impact the absolute values at high and low frequencies. Therefore, $Y_{\mathrm{rms}}(f_{\mathrm{min}})$ stays constant. Concerning individual harmonics, also here only Y_3 is excited. This feature is not affected by a change of the double layer capacitance C_{DL}. Thus, the previously described changes of the characteristic features for Y_{rms} are similar for Y_3, as only Y_3 contributes to Y_{rms} in this case.

In the following, a variation of the exchange current density i_0 and its influence on nonlinear voltage responses is investigated. The simulation results for Y_{rms} are shown in Figure 6a. With decreasing exchange current density i_0, nonlinear voltage responses increase nonlinearly, as well indicated by $Y_{\mathrm{rms}}(f_{\mathrm{min}})$. Further, the

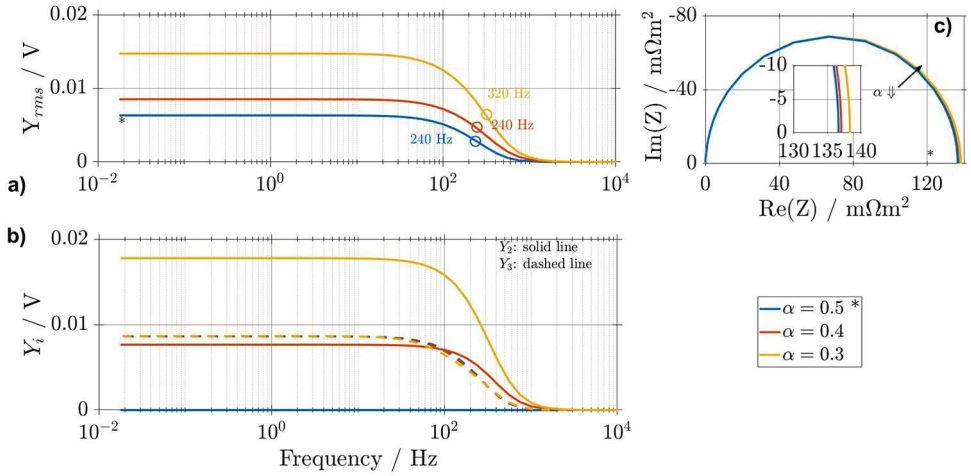

Fig. 7. Simulated NFR for the reaction model with a variation of the symmetry factor α for (a) Y_{rms}, (b) individual harmonics Y_2 and Y_3 and (c) EIS. The reference case simulation with parameters from Table 1 is marked with an asterisk.

characteristic turning point as well as f_{min} and f_{max} move towards lower frequencies. For an increase of the exchange current density i_0 this is vice versa. This can analogously be observed for the impedance in Figure 6c. A shift of the characteristic frequency towards lower frequencies and a higher impedance in general indicates a slower process with a higher resistance i.e for a lower exchange current density i_0. Concerning individual harmonics, again, only the third harmonic Y_3 is excited and therefore changes of the characteristic feature of Y_3 are again, similar to Y_{rms}. Overall, the information accessed by NFRA and EIS for a variation of the exchange current density i_0 is comparable.

In the following, the influence of the symmetry of the electrochemical reaction on NFRA by a variation of the symmetry factor α is investigated. In general, decreasing and increasing the symmetry factor by a certain value with reference to 0.5 will lead to the same excitation of higher harmonics as shown in the Appendix A for $\alpha = 0.4$ and $\alpha = 0.6$. Therefore, focus is laid on decreasing of the symmetry factor α. A decreasing symmetry factor α leads to higher nonlinear voltage responses, as shown in Figure 7a by an increased $Y_{\mathrm{rms}}(f_{\mathrm{min}})$. In combination with the simulation in the Appendix A it can be concluded that not the absolute value of α determines the excitation of higher harmonics but its deviation from 0.5.

An investigation of the individual harmonics Y_2 and Y_3 shows that voltage responses of the third harmonic Y_3 are barely affected by a change of the symmetry factor, but as soon as the reaction becomes asymmetrical for $\alpha \neq 0.5$, Y_2 is excited. It has a similar curve shape with a constant but alpha-dependent value $Y_2(f_{\mathrm{min}})$ at low frequencies and a smooth decrease to zero at higher frequencies greater than f_{max}. This characteristic information cannot be accessed by EIS, shown in Figure 7c, where a decreasing symmetry factor α only leads to a minorly increased semi-circle corresponding to an increased linear output as for a priorly observed decreased exchange current density i_0. The excitation of Y_2 further causes the turning point of Y_{rms} and the characteristic frequencies to move to higher frequencies, if α is smaller than 0.4.

For a variation of the symmetry factor α, a significant advantage of NFRA compared to conventional EIS can be observed, a symmetry change causes a specific excitation of the second harmonic Y_2. This phenomenon is further investigated in the following.

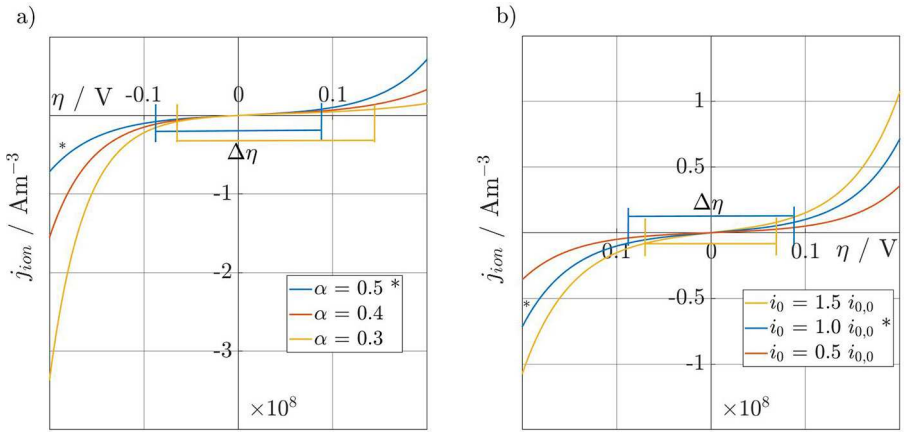

Fig. 8. Butler-Volmer kinetics for (a) variation of symmetry factor α and (b) exchange current density i_0 with reference values according Table 1. The reference case is marked with an asterisk.

In Figure 8a, the change of the current voltage relation according to the Butler-Volmer equation due to a change of α is shown. Additionally, the maximal overpotentials $\Delta\eta$ which are excited for the reference case and for $\alpha = 0.5$ are shown. For a perfectly symmetric reaction, with $\alpha = 0.5$, only Y_3 is excited and η changes symmetrically around 0. If α is decreased, the corresponding curve changes its characteristic progression and becomes asymmetrical, as shown in Figure 8a. The slope increases on the left hand side of the y-axis and decreases on the corresponding right hand side. This causes a shift of the mean overpotentials and $\Delta\eta$ to the right for a decreased α, thereby leading to an excitation of Y_2. This unique feature of NFRA suggests that NFRA might also allow to determine α without recording current voltage curves.

In Figure 8b, the change of the current voltage relation according to the Butler-Volmer equation for a change of the exchange current density i_0 is shown for comparison. Again, maximal overpotentials $\Delta\eta$ for the reference case and the deviation from it are shown. With increasing i_0, the slope of the plotted curve becomes steeper. Both, curve and $\Delta\eta$ stay symmetrical to the potential of 0, making a change in i_0 distinguishable from that of α. Both, oxidation and reduction current, lead to a smaller $\Delta\eta$ to the higher j_f generation. This explains the decrease of impedance and NFR for a larger exchange current density i_0, as shown in Figure 6. If i_0 is lowered, the observed effects are vice versa.

We aim to understand the excitation of the second Y_2 and third Y_3 harmonic in general, as it is an important feature of NFR spectra. Usually, a sinusoidal current (blue curve) is applied to the model, as shown in the following equation.

$$I = I_{\mathrm{AC}} \sin(2\pi f t),$$

with the frequency f. As a result, the full range of the symmetric Butler-Volmer curve is employed, resulting in positive and negative potentials. If instead only a partial sinusoidal excitation (yellow curve) is periodically applied to the model, as shown in the following equation, only one branch of the Butler-Volmer equation is employed, resulting in a correlation of current and potential which is not symmetric to $\mathrm{i} = 0, \eta = 0$ any more.

$$I = I_{\mathrm{AC}} || \sin(2\pi f t) || > 0.$$

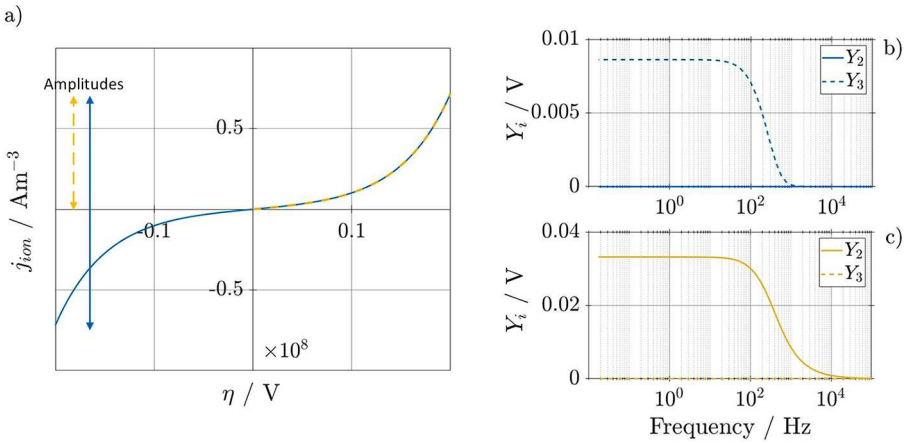

Fig. 9. Correlation between shape of current excitation and higher harmonics Y_2 and Y_3 with (a) Butler-Volmer kinetics with full (solid) and partial (dashed) sinusoidal excitation of current, (b) individual harmonics for sinusoidal excitation and (c) individual harmonics for partially sinusoidal excitation.

This could be the case for completely irreversible reaction or operation with additional DC current. In Figure 9b, individual harmonics Y_2 and Y_3 for the sinusoidal excitation of the system are shown. This results in the well known excitation of Y_3. In Figure 9c, individual harmonics Y_2 and Y_3 for the partially sinusoidal excitation of the system are shown. We see that in this case only the second harmonic Y_2 is excited. This leads to the conclusion that a nonlinear relation between current and potential which is symmetric to the center causes an excitation of the third harmonic Y_3 and a nonlinear relation between current and potential which is symmetric to the y-axis or which has only positive current and voltage causes an excitation of Y_2. This can be explained with the different parities of the harmonics. Additionally, the excitation of harmonics is not linear since the maximal amplitude of Y_2 is three times as high as the corresponding maximal amplitude of Y_3. For real systems, the relation between current and potential will neither be fully symmetric to the center nor to the y-axis and therefore an excitation of both individual harmonics, Y_2 and Y_3, will both be present, as found in our previously published experimental studies [7,8].

Finally, the influence on NFRA for operating a cell under load is investigated by adding a DC excitation. In Figure 10a, Y_{rms} is shown. If an additional DC is applied to the system, Y_{rms} increases nonlinearly and the turning point as well as f_{max} and f_{min} shift slightly towards higher frequencies. Overall, NFR are excited in the same frequency range, but with a higher overall value, again indicated by $Y_{\mathrm{rms}}(f_{\mathrm{min}})$, as well. To understand this behavior, individual harmonics, shown in Figure 10b, are investigated. With increasing DC current, the operating point shifts farther away from the symmetry point at zero current on the Butler-Volmer curve in Figure 8, and the current oscillates symmetrically around this new value, leading to strong asymmetric current-voltage relation. Therefore, the second harmonic Y_2 is excited. In parallel, the voltage responses of Y_3 decrease. A DC current equals an offset concerning the current j_{f} in the Butler-Volmer equation and due to the exponential relation between current and potential, a smaller overall change in potential results. Thereby, the linear output and Y_3 decrease. These findings are confirmed by investigation of EIS, shown in Figure 10c, where the corresponding semi-circle becomes slightly smaller with increasing DC current. The characteristic frequency is barely

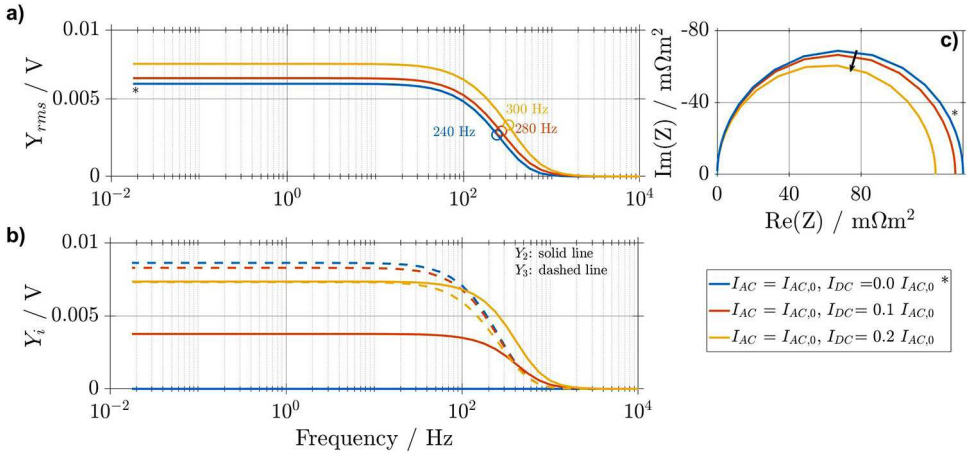

Fig. 10. Simulated NFR for reaction model and DC excitation of the cell for (a) Y_{rms}, (b) individual harmonics Y_2 and Y_3 and (c) EIS. The reference case simulation with parameters from Table 1 is marked with an asterisk.

influenced, indicated by the black arrow. Also here, we can clearly see that the single higher harmonics yield more information than EIS.

4.2 Comparison of parameter effects

In this section, the quantitative and qualitative impact of the various investigated parameters on NFR spectra is compared using the characteristic NFRA values f_{min}, f_{max} and $Y_{\mathrm{rms}}(f_{\mathrm{min}})$. As priorly discussed, the characteristics f_{min} and f_{max} are used for separation and characterization of process-dependent NFRA frequency regions, and $Y_{\mathrm{rms}}(f_{\mathrm{min}})$ represents the constant Y_{rms} values in the lowest frequency range. In case that f_{min} and f_{max} are both higher, or lower than the reference value, the reaction process becomes faster, or slower for the corresponding variation of the model parameter, respectively. In the bar plots in Figures 11, 12 and 13, the values of the characteristics relative to the reference case, i.e. $f_{\mathrm{min}}/f_{\mathrm{min,0}}$, $f_{\mathrm{max}}/f_{\mathrm{max,0}}$ and $Y_{\mathrm{rms}}(f_{\mathrm{min}})/Y_{\mathrm{rms}}(f_{\mathrm{min,0}})$ are given. Thus, the values of the reference case are 1 and marked with a dashed line in the corresponding figures.

It can be seen that for the investigated reaction, a variation of parameters has a strong influence on the characteristics. If the excitation amplitude I_{AC} is increased, all characteristics are increased. The higher amplitudes cause a larger deviation from linear current potential relation and thus stronger nonlinearities. Also, for higher amplitudes, the double layer is charged faster, leading to a faster increase in voltage and reaction and thus to higher frequencies. This impact is vice versa for a decreasing excitation amplitude: $Y_{\mathrm{rms}}(f_{\mathrm{min}})$ has a lower value, the NFR slope is flatter and f_{min} and f_{max} are at lower frequencies.

A change of the double layer capacitance C_{DL} does not affect the intensity of NFR and therefore, the absolute value $Y_{\mathrm{rms}}(f_{\mathrm{min}})$ stays constant at the reference value for each variation of the double layer capacitance. However, the frequency characteristics shift as C_{DL} determines the time delay between current and voltage or reaction. For an increase of C_{DL}, the frequencies f_{min}, respectively f_{max}, are at lower frequencies, and thus the reaction process becomes slower.

A variation of the exchange current density i_0, again, influences all characteristics. For increasing the exchange current density i_0 in comparison to the reference case,

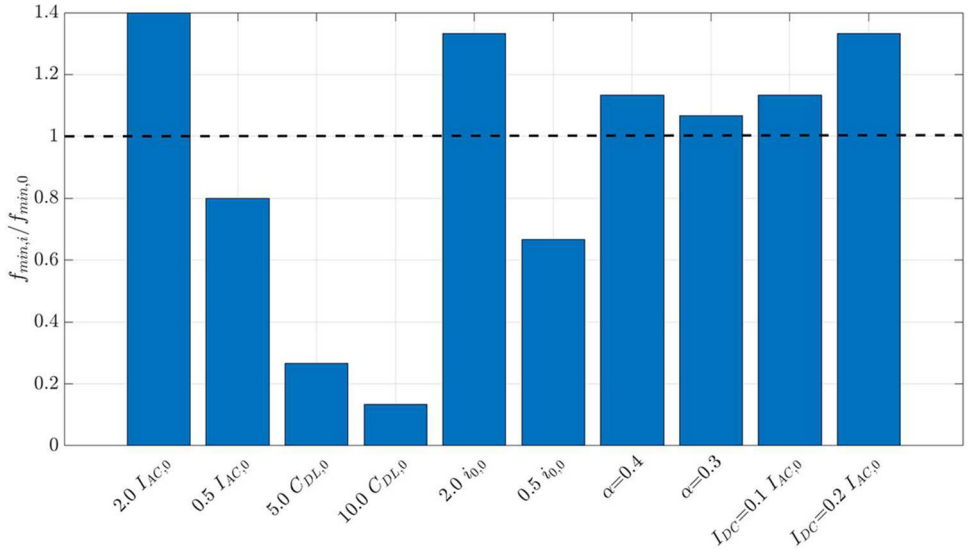

Fig. 11. $f_{\min}$ relative to the reference case gathered from tangent method; the reference case simulation is marked with a dashed line with parameters from Table 1.

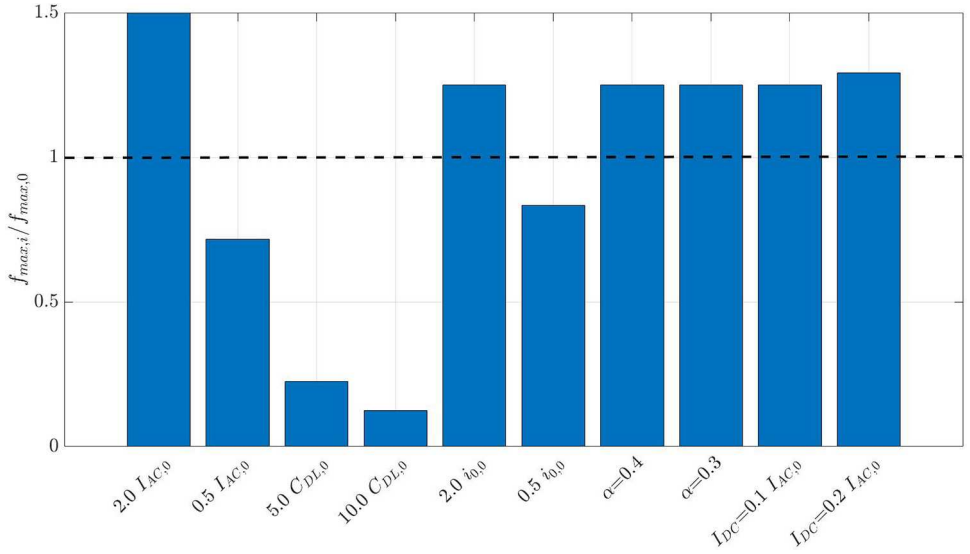

Fig. 12. $f_{\max}$ relative to the reference case gathered from tangent method; the reference case simulation is marked with a dashed line with parameters from Table 1.

the overall excited nonlinearities Y_{rms} are lower, as less overpotential is required for the same reaction current. As the reaction can follow current more easily also for fast charges, $f_{\min}$ and $f_{\max}$ shift to higher values. Adding an additional DC current impacts all characteristics. Both parameters increase the overall excitation of nonlinearities Y_{rms} due to the respective change of symmetry and therefore a corresponding excitation of Y_2. Thus, the slope of NFR between the characteristic frequencies $f_{\min}$ and $f_{\max}$ is steeper, which shifts these characteristics to higher frequencies.

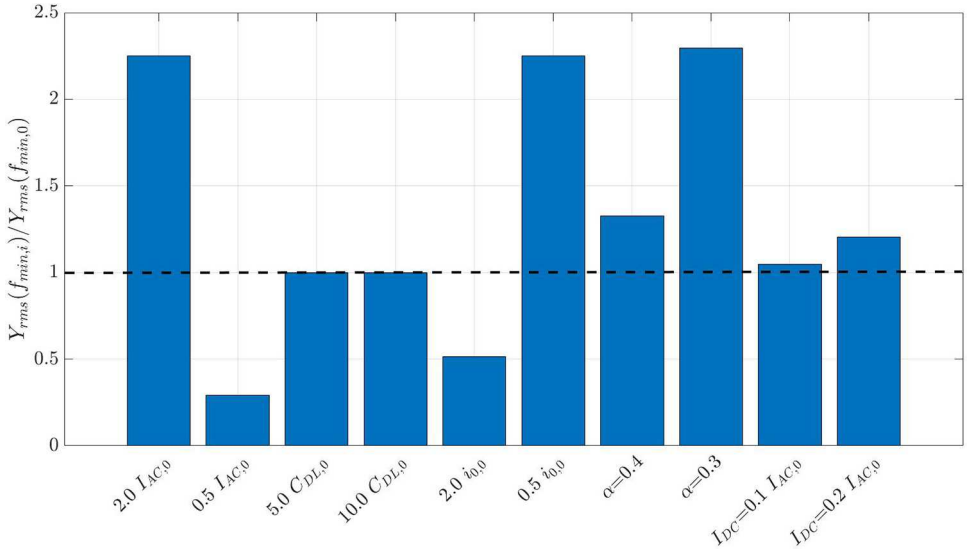

Fig. 13. $Y_{\mathrm{rms}}(f_{\mathrm{min}})$ relative to the reference case gathered from tangent method; the reference case simulation is marked with a dashed line with parameters from Table 1.

For a variation of the symmetry factor α, the reaction process changes its symmetry and becomes asymmetric compared to the reference case. Thereby, due to the previously discussed reasons, higher nonlinearities are excited and the corresponding $Y_{\mathrm{rms}}(f_{\mathrm{min}})$ has a higher value. Both characteristics f_{min} and f_{max} are sensitive to change of the symmetry factor. However, f_{min} is slightly more sensitive to a lowering of the symmetry factor than f_{max}. Here, $Y_{\mathrm{rms}}(f_{\mathrm{min}})$ is the most impacted characteristic.

To conclude, NFRA characteristics identified in this section using the tangent method are highly sensitive to parameter variations. The given overview should aid future studies in understanding and identifying the reason for experimentally observed changes in NFR spectra. Vice versa, NFR might even be a proper tool of material scientists to tailor certain material properties.

4.3 Impact of diffusion

As the previous section has clearly shown, the impact of reaction on the nonlinear response of the cell and how to interpret the spectra, we now focus on the second most important process, diffusion. We investigate the excitation of higher harmonics due to planar and spherical diffusion. At this point, only the impact of sinusoidal current on open circuit potential via consumption or production of species is analyzed, as described in Section 3.2. For the full impact of diffusion on open circuit and overpotential we refer to the next section of the coupling of diffusion and reaction. Please note that we define spherical diffusion as our reference case.

First, impedance spectra for the different diffusion processes and for different diffusion coefficients are shown in Figure 14. Simulated impedance spectra show characteristic, well known behavior from the literature [10] for the chosen boundary conditions. The models with planar diffusion, with the reference and for a significantly lowered diffusion coefficient, both show the typical slope of 45° at least at low frequencies, as observed by Jacobsen et al. for a planar blocking diffusion impedance [10]. By decreasing the diffusion coefficient, diffusion slows down, causing a higher impedance at all frequencies. This is observed for spherical diffusion, as well. Spherical

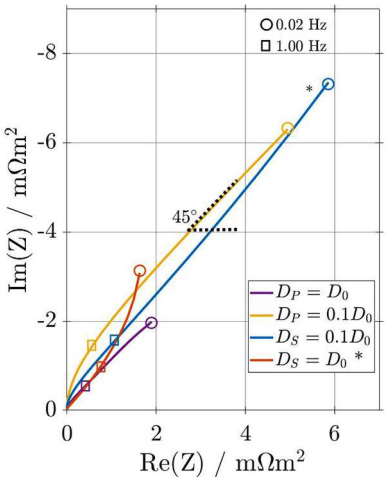

Fig. 14. Simulated impedance spectra for planar and spherical diffusion for different diffusion coefficients D_S, D_P. The reference case simulation for spherical diffusion with parameters from Table 1 is marked with an asterisk.

diffusion leads to a steeper slope than planar diffusion, which is explained in-depth in the next paragraph and observed by Jacobsen et al. for a spherical blocking diffusion impedance [10]. Further, for the reference case, a transition towards capacitative behavior is visible. If the frequency was decreased further, ideal capacitative behavior would occur. By decreasing the diffusion coefficient by 90%, this transition is moved to even lower frequencies, not visible in the spectrum. This interpretation is supported by the characteristic time constants:

$$\tau = \frac{d^2}{D}, \tag{16}$$

with d being the characteristic length from Table 1. It can be seen, that a decreasing diffusion coefficient leads to a higher time constant and therewith a smaller characteristic frequency.

In Figure 15, nonlinear voltage responses for planar and spherical diffusion are shown. The tangent method can not be applied to analyze the obtained NFR spectra, as NFR excited by diffusion do not have the same characteristic progression as NFR excited by a reaction process.

Concerning Y_{rms}, in Figure 15a, no distinct maximum nor turning point is visible, only a continuous, increase of exponential shape of NFR with decreasing frequency can be observed, starting at a frequency of ca. 0.4 Hz. Therefore, neither $f_{\max}$ nor $f_{\min}$ can be determined. Overall, a lower frequency range compared to the reaction process is excited. The characteristic time constant according to equation (16) is at 200 s corresponding to 0.005 Hz, which indicates that nonlinear responses due to diffusion will be indeed rather in the mHz range only. Diffusion coefficients are in the order of $10^{-12}\,\mathrm{m^2\,s^{-1}}$ and therefore lead to a small concentration change, resulting in small $\Delta\phi^0$ changes and therewith NFR amplitudes. Nonlinear voltage responses are higher for spherical diffusion compared to planar diffusion as explained in the following. Within the underlying model, spherical and planar diffusion are assumed to have the same surface area. The diffusion area within a sphere becomes smaller towards the inner radius and therefore results in a nonlinear concentration profile during steady state in the particle due to less diffusive transport than in the planar case. Here, with

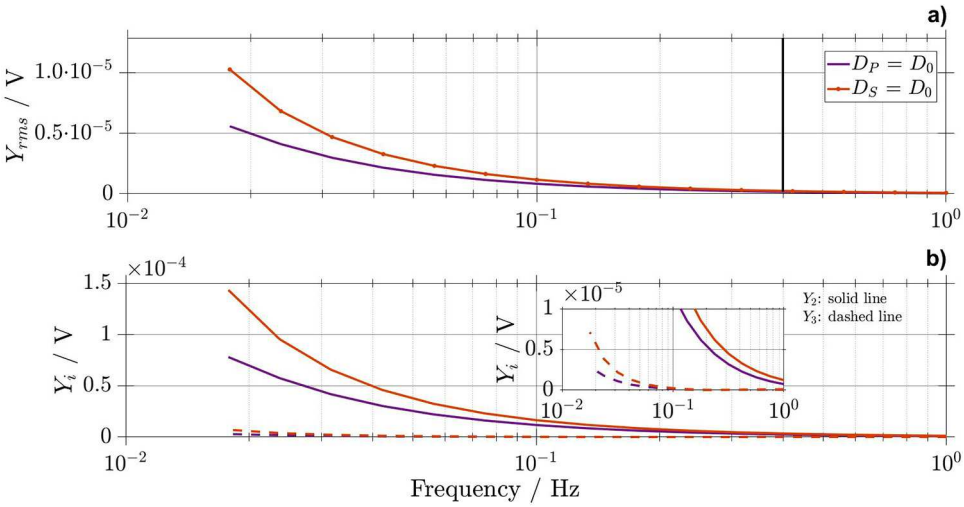

Fig. 15. Simulated NFR for planar and spherical diffusion for (a) Y_{rms} with a marker (black line) for the lowest frequency with higher harmonic excitation and (b) individual harmonics Y_2 and Y_3, with the reference case simulation parameters from Table 1.

a uniform diffusion path across the overall thickness and the uniform diffusion area itself, a linear concentration profile and higher molar flows at steady state occurs. This leads to higher nonlinear voltage responses for the spherical compared to the planar diffusion process.

In Figure 15b, individual harmonics Y_2 and Y_3 are shown. Y_2 is thereby more sensitive than Y_3 (additionally shown in the inlet) for both diffusion processes. This corresponds to the findings of the reaction model, where concentration impact excites Y_2 more than Y_3.

4.4 Impact of coupled reaction and diffusion

In a last step, the impact of both, reaction and diffusion, is investigated and simulation results are shown in Figure 16. Here, the model derived in Section 3 without further simplifications and including concentration dependent reaction rate, as described in Section 3.3 is used.

For Y_{rms}, shown in Figure 16a, a superposition of the priorly analyzed impacts of reaction and diffusion processes can be seen. At high frequencies, the curve is identical to the spectrum for the reaction process in Figure 4a, as it can be seen by identical values of f_{min}, f_{max} and the corresponding turning point. For lower frequencies, the signal shows, in addition the typical exponential increase due to diffusion effects (see Fig. 15). In general, nonlinear voltage responses are significantly higher in the low frequency domain, if diffusion is coupled with a reaction process compared to solely investigating the diffusion process. Within the model for quantifying the diffusion impact only its impact on $\Delta\phi^0$ was investigated. When taking into account that most reaction kinetics and thus, η is concentration dependent, this has a strong impact on nonlinearities. It significantly increases nonlinearities in the system by a factor of 100 at the diffusion-dominated low frequency range, showing the dominant impact of diffusion kinetics, i.e. η compared to thermodynamics, i.e. $\Delta\phi_{\mathrm{OCP}}$.

If individual harmonics are investigated, shown in Figure 16b, these findings are confirmed. In general, Y_2 and Y_3 are excited by the coupled processes. Y_3 thereby

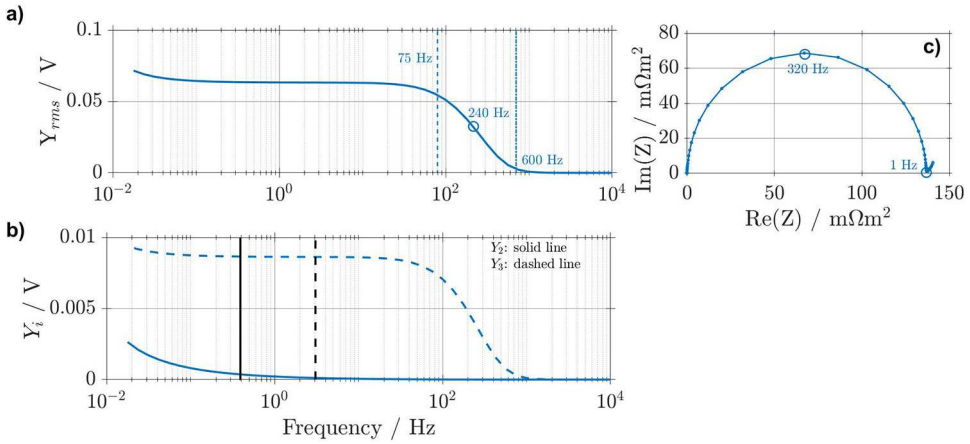

Fig. 16. Simulated NFR for reaction with a coupled diffusion process for (a) Y_{rms} f_{min} is marked by a dashed blue line and f_{max} is marked by a dash-dotted blue line, (b) individual harmonics Y_2 and Y_3 with markers for the beginning of the excitation of the priorly investigated diffusion process (solid black line) and the corresponding frequency of the coupled model (dashed black line) and (c) EIS. Reference case simulation parameters from Table 1 are used.

dominates the overall frequency range and is excited at high frequencies due the reaction process. Since the reaction process is symmetrical at these frequencies due to a quasi steady-state activity of one, Y_2 is not affected at this point. This corresponds to the discussion of the excitation of higher harmonics due to a singular reaction process, shown in Section 4.1. Y_2 is excited at lower frequencies, similar as for the investigation of the diffusion process, shown in Section 4.3. Nevertheless, the amplitude for the excitation of higher harmonics in the diffusion dominated frequency range is significantly higher, thereby confirming the previously mentioned dependency of η of the concentration in this frequency range. Additionally, Y_2 is excited starting at a frequency still characteristic for the reaction, which shows the impact of diffusion on overpotential. The solid black line thereby indicates the beginning of higher harmonic voltage excitation due to the priorly observed diffusion process in scenario 2. It is at lower frequencies than the dashed black line, which marks the onset of higher harmonic voltage excitation of Y_2 for the coupled model. Y_3, however, is less affected from diffusion than Y_2.

In the impedance spectrum, in Figure 16c, a semi-circle for the reaction process with a maximum at 320 Hz and a branch in the low frequency range on the right hand side of the spectrum for the diffusion process, beginning at 1 Hz, are visible, confirming the shown impacts of diffusion at low frequencies.

With these results, the occurrence of Y_2 as well as Y_3 in experimental studies on Lithium-ion batteries [7,8] can be explained, as in battery cells electrochemical reaction and diffusion process are always inevitably coupled.

5 Conclusions

Prior research showed that Nonlinear Frequency Response Analysis (NFRA) is a powerful, but yet seldomly used tool for the in-depth study of processes in electrochemical cells and electrodes and for diagnosing cell states. The here presented work aims to deliver a basic guideline to enhance interpretation and usage of NFRA via

illustrating the nonlinearity using simple fundamental models. The effect of fundamental processes in electrochemical cells on NFR spectra is first analyzed using a basic electrochemical reaction. Subsequently, the often encountered limited reactant availability, i.e. diffusion, is analyzed, and its impact on NFRA is shown. Then the interaction of both processes is revealed.

Focus is thereby laid on understanding why and how individual harmonics are excited by variation of the input amplitude I_{AC}, double layer capacitance C_{DL}, exchange current density i_0 and symmetry factor α. We show that exciting a system sinusoidally around an operating point, which shows point symmetry in the nonlinear current voltage relation causes the excitation of the third harmonic Y_3. This is typically achieved when operating at zero current for a Butler-Volmer kinetics with $\alpha = 0.5$. By changing α or applying a current, we can generate an excitation of Y_2. NFRA thus yields essential information about the kinetics, which can not be accessed by conventional methods, such as EIS. Bar plots summarize the findings and give an overview on how and where each kinetic and electrode parameter impacts the spectrum.

Additionally, we showed that planar and spherical solid diffusion cause an excitation of both individual harmonics Y_2 and to less extend Y_3 at low frequencies. Thereby, the relation between current and concentration is purely linear and not exciting higher harmonics. Only due to the nonlinear relation between concentration and potential, higher harmonics are excited. Spherical diffusion was shown to cause higher nonlinearities.

Finally, a coupled simulation of reaction and diffusion was shown to be a superposition of both signals, with diffusion dominating in the low frequency range and reaction in higher frequencies. Additionally, a significant increase for Y_2 beginning at frequencies still characteristic for the reaction process can be observed.

As experimental EIS measurement devices often already have the option of NFRA included, we hope to encourage with this work a widespread application of this promising technique not only for fundamental analysis of kinetic processes at electrodes, but also for state estimation of cells. The latter is especially interesting for Lithium-ion battery research, where estimation of State-of-Health and State-of-Charge of full cells as well as the kind of ageing is essential but yet cumbersome.

Author contribution statement

Ulrike Krewer is the corresponding author of the paper and further significantly contributed to the scientific output of this research with model formulation, case study selection, in-depth discussions on electrochemistry and NFRA interpretation. Marco Heinrich contributed to the paper with in-depth discussions about the simulated results. Fridolin Röder provided assistant modeling and interpretation of simulated results. Nina Harting helped, in very close collaboration, with the interpretation of the simulated results and by further writing parts of the introduction. Without her years of expertise in expertise of in the experimental field of NFRA a scientific output with significance would not have been possible. Nicolas Wolff, as a first author, wrote all further parts of the paper and provided the models and performed the simulations.

Appendix A

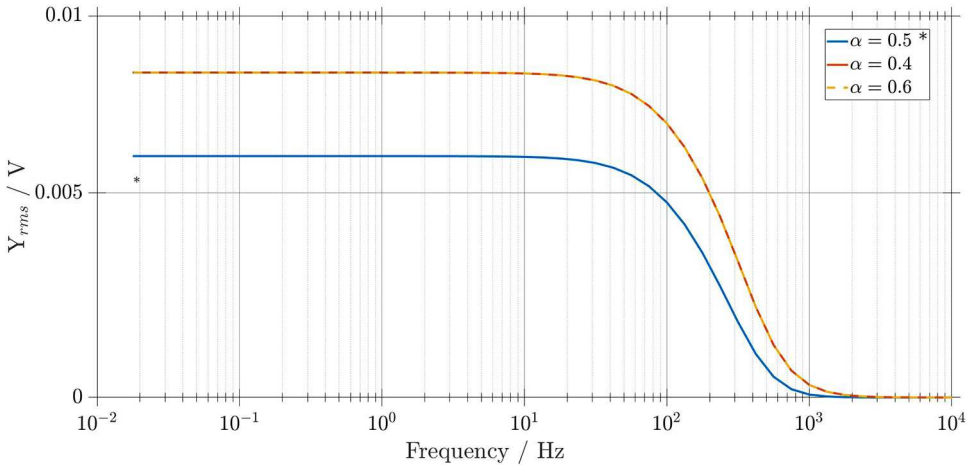

Fig. A1. Simulated NFR for the reaction model with a variation of the symmetry factor α for Y_{rms}. The reference case simulation with parameters from Table 1 is marked with an asterisk.

List of symbols

a_s	Specific surface area, m^{-1}
A	Area, m^2
A	Reactant, –
A^+	Oxidized reactant, –
a_A	Activity of reactant A, –
c_A	Species concentration, mol m^{-3}
$c_{A,0}$	Standard equilibrium concentration, mol m^{-3}
C_{DL}	Double layer capacity, C m^{-2}
d	Diffusion length, m
D	Diffusion coefficient, m^2 s^{-1}
$\Delta\phi$	Potential gradient across the interface, V
$\Delta\phi^0$	Open circuit potential, V
$\Delta\phi^{00}$	Standard potential, V
f	Frequency, s^{-1}
f_{min}	Characteristic minimal frequency, s^{-1}
f_{max}	Characteristic maximal frequency, s^{-1}
F	Faraday constant, C mol^{-1}
Y	Voltage response, V
Y_{rms}	Root mean square of voltage response , V
i_0	Exchange current density, A m^{-2}
I_{AC}	AC current density, A
j_{f}	Faradaic volumetric reaction current, A m^{-3}
j_{tot}	Total volumetric current, A m^{-3}
n	Numerator for higher harmonic voltage responses
R	Ideal gas constant, J mol^{-1} K^{-1}
R	Particle radius, m

r	Radial coordinate, m
t	Time, s
T	Temperature, K
T_P	Turning point,
v_j	Discrete function value, V
x	Spacial coordinate, m
z	Number of sample points, –
α	Reaction symmetry factor, –
ε	Volume fraction, –
η	Reaction overpotential, V
ϕ	Electrical potential, V

References

1. D. Andre, M. Meiler, K. Steiner, Ch. Wimmer, T. Soczka-Guth, D.U. Sauer, J. Power Sources **196**, 5334 (2011)
2. H. Baltruschat, Am. Soc. Mass Spectr. **15**, 1693 (2004)
3. A.J. Bard, L.R. Faulkner, E. Swain, C. Robey, *Electrochemical Methods: Fundamentals and Applications* (John Wiley & Sons, 2001)
4. B. Bensmann, M. Petkovska, R. Hanke-rauschenbach, K. Sundmacher, J. Electrochem. Soc. **157**, 1279 (2010)
5. D.M. Bernardi, J. Go, J. Power Sources **196**, 412 (2011)
6. N. Elgrishi, K.J. Rountree, B.D. Mccarthy, E.S. Rountree, T.T. Eisenhart, J.L. Dempsey, J. Chem. Educ. **95**, 197 (2018)
7. N. Harting, N. Wolff, U. Krewer, Electrochim. Acta **281**, 378 (2018)
8. N. Harting, N. Wolff, F. Röder, U. Krewer, Electrochim. Acta **248**, 133 (2017)
9. J. Heinze, Angew. Chem. **23**, 831 (1984)
10. T. Jacobsen, K. West, Electrochim. Acta **40** (1995)
11. T. Kadyk, R. Hanke-Rauschenbach, K. Sundmacher, J. Electroanal. Chem. **630**, 19 (2009)
12. T. Kadyk, R. Hanke-Rauschenbach, K. Sundmacher, J. Appl. Electrochem. **41**, 1021 (2011)
13. T. Kadyk, R. Hanke-rauschenbach, K. Sundmacher, Int. J. Hydrogen Energy **37**, 7689 (2012)
14. M. Kiel, O. Bohlen, D.U. Sauer, Electrochim. Acta **53**, 7367 (2008)
15. M. Koper, J. Chem. Soc. Faraday Trans. **94**, 1369 (1998)
16. J. Koryta, J. Dvorak, V. Bohackova, *Lehrbuch der Elektrochemie* (Springer Verlag, 2012)
17. U. Krewer, A. Kamat, K. Sundmacher, J. Electroanal. Chem. **609**, 105 (2007)
18. U. Krewer, T. Vidakovic-Koch, L. Rihko-Struckmann, ChemPhysChem **12**, 2518 (2011)
19. F. Kubannek, U. Krewer, Electrochim. Acta **210**, 862 (2016)
20. Q. Mao, U. Krewer, Electrochim. Acta **68**, 60 (2012)
21. Q. Mao, U. Krewer, Electrochim. Acta **103**, 188 (2013)
22. Q. Mao, U. Krewer, R. Hanke-Rauschenbach, Electrochem. Commun. **12**, 1517 (2010)
23. M.D. Murbach, D.T. Schwartz, J. Electrochem. Soc. **164**, 3311 (2017)
24. H. Ramon, E. Siller, Non-Linear Modal Analysis Methods for Engineering, PhD thesis, Imperial College London, 2004
25. J. Rusling, S.L. Suib, Adv. Mater. **6**, 922 (1994)
26. H. Schweiger, O. Obeidi, O. Komesker, A. Raschke, M. Schiemann, C. Zehner, M. Gehnen, M. Keller, P. Birke, Sensors **10**, 5604 (2010)
27. H. Varela, K. Krischer, Catal. Today **70**, 411 (2001)
28. T.R. Vidakovic-Koch, V.V. Panic, M. Andric, M. Petkovska, K. Sundmacher, J. Phys. Chem. C **115**, 17341 (2011)

29. T.R. Vidakovic-Koch, V.V. Panic, M. Andric, M. Petkovska, K. Sundmacher, J. Phys. Chem. C **115**, 17352 (2011)
30. J.R. Wilson, D.T. Schwartz, S.B. Adler, Electrochim. Acta **51**, 1389 (2006)
31. N. Wolff, N. Harting, M. Heinrich, F. Röder, U. Krewer, Electrochim. Acta **260**, 614 (2018)